Acta Crystallographica Section D
Biological Crystallography
ISSN 0907-4449

Structural consequences of hen egg-white lysozyme orthorhombic crystal growth in a high magnetic field: validation of X-ray diffraction intensity, conformational energy searching and quantitative analysis of *B* factors and mosaicity

Shinya Saijo,[a] Yusuke Yamada,[a] Takao Sato,[a]* Nobuo Tanaka,[a] Takuro Matsui,[b,c] Gen Sazaki,[b,c] Kazuo Nakajima[b] and Yoshiki Matsuura[d]

[a]Depertment of Life Science, Graduate School of Bioscience and Biotechnology, Tokyo Institute of Technology, 4259-B-10 Nagatsuta, Midori-ku, Yokohama 226-8501, Japan, [b]Institute for Materials Research, Tohoku University, Sendai 980-8577, Japan, [c]Center for Interdisciplinary Research, Tohoku University, Sendai 980-8578, Japan, and [d]Institute for Protein Research, Osaka University, 3-2 Yamadaoka, Suita, Osaka 565-0871, Japan

Correspondence e-mail: tsatoh@bio.titech.ac.jp

Received 9 July 2004
Accepted 25 November 2004

PDB References: 0 T HEWL, 1wtm, r1wtmsf; 10 T HEWL, 1wtn, r1wtnsf.

A novel method has been developed to improve protein-crystal perfection during crystallization in a high magnetic field and structural studies have been undertaken. The three-dimensional structure of orthorhombic hen egg-white (HEW) lysozyme crystals grown in a homogeneous and static magnetic field of 10 T has been determined and refined to a resolution of 1.13 Å and an *R* factor of 17.0%. The 10 T crystals belonged to space group $P2_12_12_1$, with unit-cell parameters $a = 56.54$ (3), $b = 73.86$ (6), $c = 30.50$ (2) Å and one molecule per asymmetric unit. A comparison of the structures of the 0 T and 10 T crystals has been carried out. The magnitude of the structural changes, with a root-mean-square deviation value of 0.75 Å for the positions of all protein atoms, is similar to that observed when an identical protein structure is resolved in two different crystalline lattices. The structures remain similar, with the exception of a few residues *e.g.* Arg68, Arg73, Arg128 and Gln121. The shifts of the arginine residues result in very significant structural fluctuations, which can have large effects on a protein's crystallization properties. The high magnetic field contributed to an improvement in diffraction intensity by (i) the displacement of the charged side chains of Arg68 and Arg73 in the flexible loop and of Arg128 at the C-terminus and (ii) the removal of the alternate conformations of the charged side chains of Arg21, Lys97 or Arg114. The improvement in crystal perfection might arise from the magnetic effect on molecular orientation without structural change and differences in molecular interactions. X-ray diffraction and molecular-modelling studies of lysozyme crystals grown in a 10 T field have indicated that the field contributes to the stability of the dihedral angle. The average difference in conformational energy has a value of -578 kJ mol^{-1} per charged residue in favour of the crystal grown in the magnetic field. For most protein atoms, the average *B* factor in the 10 T crystal shows an improvement of 1.8 Å^2 over that for the 0 T control; subsequently, the difference in diffraction intensity between the 10 T and 0 T crystals corresponds to an increase of 22.6% at the resolution limit. The mosaicity of the 10 T crystal was better than that of the 0 T crystal. More highly isotropic values of 0.0065, 0.0049 and 0.0048° were recorded along the *a*, *b* and *c* axes, respectively. Anisotropic mosaicity analysis indicated that crystal growth is most perfect in the direction that corresponds to the favoured growth direction of the crystal, and that the crystal grown in the magnetic field had domains that were three times the volume of those of the control crystal. Overall, the magnetic field has improved the quality of these crystals and the diffracted intensity has increased significantly with the magnetic field, leading to a higher resolution.

1. Introduction

In the race to solve and understand new structures using structural genomics, crystal-optimization techniques should be given high priority, but this is not always the case in the funding programmes of various countries. An exciting procedure that has shown very good potential is the use of a strong magnetic field for crystallization, which leads to the production of a smaller number of higher quality crystals. This effect is anticipated to produce crystals that have a higher diffraction intensity under conditions where protein crystallization is facilitated by a high magnetic field of 10 T. It has been shown that a high magnetic field enhances the perfection of protein crystals (Lin *et al.*, 2000; Sato *et al.*, 2000, 2001, 2002, 2004; Astier *et al.*, 2001; Ataka & Wakayama, 2002), leading to an increase in the maximum resolution of X-ray diffraction. This effect can be attributed to a slowing of the growth rate caused by magnetic damping of convection in the solution (Sazaki *et al.*, 1999; Zhong & Wakayama, 2001) and/or by the diamagnetic orientation of mosaic blocks during crystal growth. The diamagnetic anisotropy of the protein molecules (Worcester, 1978) is reflected in the crystal, resulting in an oriented growth with respect to the direction of the magnetic field. In such a case, we can also expect that a Lorentz force or electromagnetic induction is operating in the crystal, causing the positions of the amino-acid side chains to deviate. The same force operating on ionic species in an electrolyte causes magnetic damping in the solution. In protein crystals that contain a sufficient amount of solvent the molecular surfaces are exposed to the solution where charged amino-acid side chains exist. These side chains are mostly charged to some extent and are very often flexible, exhibiting high thermal motion. In recent years, protein engineering of residues on the surface of a protein to side chains that have lower entropy has been harnessed to good effect, resulting for example in improved diffraction resolution (Derewenda, 2004; Czepas *et al.*, 2004; Mateja *et al.*, 2002). Moreover, in yet another approach, a microgravity-grown crystal of apocrustacyanin C1 showed improved ordering of seven amino-acid side chains on the surface of the protein in comparison with a ground control; of particular note, two of these side chains were involved in crystal lattice interactions (Habash *et al.*, 2003). However, such side chains are also likely to be affected by the magnetic field, resulting in possible movement of side chains arising from the Lorentz force and electromagnetic induction. In previous papers, we reported the characteristics of the crystallization of orthorhombic lysozyme in a 10 T magnetic field (Sato *et al.*, 2000, 2001).

We have not yet performed a broad study encompassing a number of systems. It has been reported that the technique has been used successfully for proteins other than lysozyme (Lin *et al.*, 2000; Sato *et al.*, 2002, 2004). The results of these and our studies are limited and cannot be generalized without further studies. Owing to the constraints of limited synchrotron beam time and magnet time, it was not possible to determine statistically whether the 10 T case falls outside a 0 T population distribution. However, these results indicate a significant positive effect that point towards this case and should be explored further. We now present another study that at least adds growing evidence in favour of the approach.

In this study, we have refined the crystal structures obtained at 10 and 0 T, respectively, described their comparison and quantified the effects of the high magnetic field on the quality of the lysozyme crystal in order to clarify whether it helps in obtaining better quality protein crystals that have so far resisted forming ordered arrays and to ascertain whether the effect of a magnet during crystallization is applicable to any protein or whether its use is restricted to haem proteins that contain ferromagnetic ions such as iron.

2. Experimental methods

2.1. Crystallization

The test material used for the present study was hen egg-white (HEW) lysozyme (Seikagaku Kogyo Co. Ltd, Japan). Lysozyme has long been used as the standard for protein crystal-growth research and has also been well characterized by a variety of experimental and theoretical analyses. The crystals defined here as 10 T and 0 T crystals were grown by exposing them to a high magnetic field of 10 T and a control geomagnetic field of 40 μT, respectively (Sato *et al.*, 2000). A continuous homogeneous magnetic field of 10 T was produced by a liquid-helium-free superconducting magnet (JMTD-10T100M9; Japan Magnetic Technology Inc., Tokyo, Japan). A 0.5% improved homogeneity of the field was achieved within the sample container. Orthorhombic lysozyme crystals were grown in the high magnetic field using the batch crystallization method. The crystal-growth conditions were 250 mg ml^{-1} lysozyme, 0.43 m*M* NaCl in 50 m*M* sodium acetate buffer pH 4.5 at 313 K, 11 d duration. The dimensions of the 10 T and 0 T crystals were typically 0.45 × 0.50 × 2.00 and 0.50 × 0.50 × 2.00 mm, respectively.

2.2. Experimental tests made with the sequence field on/field off

Seven crystals grown in the 10 T magnetic field were selected from those that became orientated with the field (the direction of the magnetic field corresponds to the crystallographic *c* axis). No visible crystal defects were noted. These crystals were mounted at room temperature in a 2.0 mm glass capillary with slugs of mother liquor placed at both ends and the capillary was sealed. Likewise, seven control 0 T and 10 T magnetic annealing crystals that were slightly larger in each dimension than the 10 T crystals were mounted. These crystals were divided for use in intensity measurements (see §2.3) and profile measurements (see §2.7) of the 10 T and 0 T data sets, which were performed at a wavelength of 1.000 Å. The crystals were not cryocooled but were maintained at 296 K.

The 10 T crystals were not subjected to X-ray analysis in a 10 T field; hence, it is not known precisely how the structure may differ from one that was obtained while still in the magnetic field. However, although the 0 T crystal was annealed in a 10 T field for four weeks, even a high magnetic

Table 1
Statistics of data collection.

Owing to the slightly larger volume (∼3%) of the 0 T control crystal compared with the 10 T crystal, an additional very quick pass set of imaging plates were collected, *i.e.* exposure times of 80 s for 1.5° rotation (equivalent to 64 s for 1.2° rotation) so as to capture saturated spots at low resolution.

	0 T	10 T
Crystal dimensions (mm)	0.5 × 0.5 × 2	0.45 × 0.5 × 2
Collimator diameter (mm)	0.2	0.2
Ring current (mA)	203–150	195–165
Oscillation range used per imaging plate (°)	1.5	1.2
Crystal-to-detector distance (mm)	430	430
Exposure time (s)	80	64
Total rotation collected (°)	72.0	87.6
Wavelength (Å)	1.000	1.000
Crystal system	Orthorhombic	Orthorhombic
Space group	$P2_12_12_1$	$P2_12_12_1$
Unit-cell parameters (Å)		
a	56.44 (4)	56.54 (3)
b	73.73 (7)	73.83 (6)
c	30.43 (2)	30.50 (2)
All data		
Resolution† (Å)	50–1.33 (1.38–1.33)	50–1.13 (1.16–1.13)
$\langle I\rangle/\langle\sigma(I)\rangle$†	3 (39.7)	3 (43.3)
Total observed data		
No. unique data	20095	34449
Completeness† (%)	93.6 (62.4)	99.5 (71.9)
$R_{\rm merge}$†‡ (%)	2.9 (20.7)	2.6 (32.5)
Overall *B* factor§ (Å^2)	9	6

† Values in parentheses are for the outer resolution shell. ‡ $R_{\rm merge} = \sum|I_i - \langle I\rangle|/\sum I_i$, where I_i is the measured intensity of individual reflections and $\langle I\rangle$ is the mean intensity of symmetry-related measurements of the reflection. § Overall *B* factor estimated from Wilson plot.

Table 2
$R_{\rm merge}$ and completeness of the X-ray data sets collected from HEW lysozyme crystals grown under a high magnetic field of 10 T, as well as the 0 T control case.

	0 T		10 T	
Resolution (Å)	$R_{\rm merge}$† (%)	Completeness (%)	$R_{\rm merge}$† (%)	Completeness (%)
16.0–2.87	2.8	98.1	2.1	70.4
2.87–2.27	3.1	99.9	2.3	96.6
2.27–1.99	3.6	97.6	2.6	89.5
1.99–1.81	4.5	77.7	3.2	81.3
1.81–1.68	5.3	59.0	3.5	74.4
1.68–1.58	6.6	60.3	4.3	69.5
1.58–1.50	8.5	60.5	5.1	65.9
1.50–1.43	11.6	61.2	6.4	63.1
1.43–1.38	16.0	61.7	7.8	60.3
1.38–1.33	20.7	60.6	10.2	57.9
1.33–1.28			12.8	55.7
1.28–1.23			16.6	53.3
1.23–1.19			21.4	50.8
1.19–1.16			28.6	47.0
1.16–1.13			32.5	35.8

† $R_{\rm merge} = \sum|I_i - \langle I\rangle|/\sum I_i$, where I_i is the measured intensity of individual reflections and $\langle I\rangle$ is the mean intensity of symmetry-related measurements of the reflection.

field of 10 T cannot improve the quality of crystals formed in the Earth's magnetic field. A 10 T crystal also does not appear to be stressed by removal of the high field. Thus, we believe that it is only the crystal-growth process itself that is affected by a magnetic field, as expected from the transient behaviour of a molecular-orientation effect, and thus we can speculate that the structures can be discriminated from the snapshots between 10 T and 0 T crystal forms.

2.3. Data collection and processing

X-ray data collection for HEW lysozyme crystals grown at 10 T and 0 T was carried out using a Weissenberg camera with an imaging plate on BL18B at the Photon Factory (PF), Tsukuba, Japan. Data-collection statistics are summarized in Table 1. The data were processed using *DENZO* and were scaled using *SCALEPACK* (Otwinowski & Minor, 1997). The resulting $R_{\rm merge}$ and completeness of both data sets in resolution shells are shown in Table 2. Sufficient high-resolution data have been secured for these crystals to allow the overall *B* factors of the 10 T and 0 T crystals to be estimated from a Wilson plot (using the program *TRUNCATE* from the *CCP*4 program suite). Unfortunately, some low-resolution reflections were lost owing to intensity overload.

2.4. Model refinement

The starting model for structural refinement in each case was the refined atomic coordinates (PDB code 1bgi; Oki *et al.*, 1999) of HEW lysozyme, *i.e.* the best resolution structure of the orthorhombic lysozyme refined so far (1.7 Å resolution). All water molecules were removed from this initial model. The coordinates of 0 T and 10 T after applying a final rigid-body solution from *EPMR* (Kissinger *et al.*, 1999) had *R* values of 0.230 and 0.223, respectively, over the resolution range 15–4 Å without any σ cutoff and had correlations of 0.870 and 0.875, respectively.

The model-refinement program *REFMAC* from the *CCP*4 software suite (Collaborative Computational Project, Number 4, 1994) was subsequently used to refine the atomic positions and isotropic thermal factors. Refinement of anisotropic thermal factors was also performed. During the entire refinement process, the same 10% of reflection data were used for calculation of $R_{\rm free}$. The crystallographic *R* and $R_{\rm free}$ factors are shown in Table 3. The molecular-display and map-fitting program *TURBO-FRODO* (Roussel & Cambillau, 1989) was used to examine and adjust the structure during the refinement process. Positions were visually selected for water molecules using *ARP*/*wARP* from *CCP*4. Water molecules were inserted into the models with an initial isotropic *B* factor of 30 Å^2 if they formed at least one stereochemically reasonable hydrogen bond (between 2.5 and 3.4 Å) and were above the 1.5 r.m.s. levels in the $F_o - F_c$ difference-density maps. If the electron density around a water molecule at the end of any given round of refinement was less than 1 r.m.s. level in the $2F_o - F_c$ map, then that molecule was deleted. Both structures were thus fully refined to an *R* factor and $R_{\rm free}$ of approximately 17 and 20%. The final model-refinement statistics are listed in Table 3.

2.5. *B*-factor analysis

A comparative analysis of the two crystal structures revealed that the 10 T structure remains very similar to the 0 T structure. Even though 10 T crystals were no longer in the high

magnetic field when they underwent X-ray analysis and were fully subject to undamped thermal vibration, a surprisingly low B factor for overall protein atoms of 10 T was observed of 17.8 compared with 19.5 Å^2 for the 0 T crystals. Furthermore, there was no significant impact on the slight structural changes in a protein crystal grown under a high magnetic field. Atoms were considered to be common if the distance between the atoms and those from the other structure was less than 1.0 Å, as determined using *DISTANG* included in the *CCP*4 suite (IUPAC-IUB Conventions, 1972).

An average B-factor analysis of the common atoms between the 10 T and 0 T structures was carried out using (1), where ΔB is the difference in B factor, d is the resolution, G is an occupancy factor equal to one and ΔI is the change in intensity,

$$\begin{aligned}\Delta I &= |F_{\mathrm{C,10\,T}}|^2 - |F_{\mathrm{C,0\,T}}|^2 \\ &= G_{10\,\mathrm{T}}^2 \exp(-2B_{10\,\mathrm{T}} \sin^2\theta\lambda^{-2}) - G_{0\,\mathrm{T}}^2 \exp(-2B_{0\,\mathrm{T}} \sin^2\theta\lambda^{-2}) \\ &= G^2 \exp(\Delta B/2d^2). \qquad (1)\end{aligned}$$

Owing to the difference (or reduction) in B factors of each population portion, the diffraction intensity of 10 T changes (or increases) at the maximum 1.33 Å resolution limit of 0 T (at the edge of the diffraction pattern).

2.6. Conformational analysis

The geometry search for side chains wais varied to generate a potential energy map. Version 6.1.1 of *BioMedCACheActive Site* (Fujitsu Ltd, Tokyo, Japan) was used to perform molecular-mechanics calculations in order to investigate energy conformations. The *CACheche* mechanics application implements an MM3 force field. *CACheche* can measure the potential energy of a series of conformations in order that low-energy conformations separated by high-energy barriers are easily located. These maps are generated from the potential energies of the conformations determined by a geometry search for the dihedral angles. Not every conformation is optimized (rigid map) since the energy optimization for each map point causes a variation in structure.

These molecular models were superimposed and the root-mean-square displacement (r.m.s.d.) was calculated by means of fitting using the program *TOP* included in *CCP*4. The r.m.s.d. value is used to measure how different each conformation of side chain is from the X-ray structure and to show the relationship with the change in conformational energy.

2.7. Mosaicity analysis

While the intensity-profile measurements were performed using a vertical-type four-circle diffractometer on beamline 10A at the PF in order to estimate the 'real' mosaicity values, the full-width at half maximum (FWHM) of all 56 rocking-curve profiles were evaluated using a least-squares fit to a non-linear model (Press *et al.*, 1995). The recorded intensity I was calculated for a peak that fitted the Gaussian distribution function of the equation

Table 3
Final model-refinement statistics for the 0 T control and 10 T lysozyme structures.

The error in coordinates is based on the Luzzati error estimate or the diffraction data precision indicator (DPI) values (Cruickshank, 1999).

	0 T	10 T
Resolution limits (Å)	16–1.33	16–1.13
R_{free} (%)	20.1	20.0
R factor (%)	17.3	17.0
No. reflections used ($F > 0$)	20095	34449
No. protein atoms	1001	1001
No. solvent molecules	88	116
No. Cl^- ions	1	1
R.m.s. deviations from ideality		
Bond lengths (Å)	0.008	0.005
Bond angles (°)	0.022	0.018
Chiral volume (Å^3)	0.090	0.076
Ramachandran plot details		
No. residues in favoured regions	114	116
No. residues in allowed regions	15	13
No. residues in disallowed regions	0	0
Error in coordinates in Luzzati plot (Å)	0.18	0.16
Coordinate error, Cruickshank's DPI (Å)	0.0744	0.0556
Mean B factors (Å^2)		
C^α atoms		
Main-chain protein atoms	17.9	16.4
Side-chain protein atoms	21.1	19.3
Overall protein atoms	19.5	17.8
Overall water molecules	34.6	37.8
Overall molecules	20.7	19.9

$$I = I_0 + (A/W)(\pi/2)^{1/2} \exp[2(X - X_0)^2/W^2],$$

where I_0 is the baseline offset, A is the area size of the curve to the baseline, X is the ω-scan step, X_0 is the centre of the symmetric peak and W is twice the standard deviation, 2σ, and W is defined as approximately 0.849 × FWHM. The data were fitted to several Gaussians with the assumption of a linear background.

Just as Snell *et al.* (1997) employed methods developed by Colapietro *et al.* (1992), where the IRF is defined, so each mosaicity as defined by $\eta = (\mathrm{FWHM}^2 - \mathrm{IRF}'^2)^{1/2}$ was estimated from the FWHM with a deconvolution of the instrument resolution function, IRF′ = 0.0023°, at this beamline (Sato *et al.*, 2000). Student's t test confirms that the 10 T and 0 T data statistically differ from each other at the 99.95% confidence interval with probability Pr (t-test value, $t > 7.299$) of 0.0005.

Later, Ferrer & Roth (1998) introduced an anisotropic mosaicity model given by (2), where η_h, η_k and η_l are the anisotropic components of crystal mosaicity,

$$\eta_{hkl}^{\mathrm{calc}} = (\eta_h h^2 + \eta_k k^2 + \eta_l l^2)/(h^2 + k^2 + l^2) + \eta_{\mathrm{const}}, \qquad (2)$$

where η_{const} was set to zero and h, k and l were the crystallographic directions. This anisotropic mosaicity has also been reformulated by Bellamy *et al.* (2000) and Snell *et al.* (2001, 2003). Using this model, η_h, η_k and η_l were calculated in degrees using a multivariate regression analysis of all mosaicity values estimated from all the 56 measured FWHM profiles as were previously reported by Sato *et al.* (2000). A sample coefficient of multiple determinations, R^2 (where R^2 is the data

that can be fitted with the model), of the model was calculated to describe the goodness of fit.

3. Results and discussion

3.1. Comparative analysis of the diffraction data

The diffraction limit of the lysozyme crystal, which was defined as the resolution at which the value of $I/\sigma(I)$ dropped below 2.0, improved significantly and was 1.13 Å for 10 T and 1.33 Å for 0 T. The number of reflections increased from 20 095 for 0 T to 34 449 for 10 T and the signal-to-noise ratio of the average $I/\sigma(I)$ also increased from 39.7 for 0 T to 43.3 for 10 T, a 9% increment. As the approximate illuminated volume ranged from 0.018 to 0.02 mm^3 using a beam size of 0.2 × 0.2 mm, although the crystal volume of 10 T is reduced by 11% compared with that of 0 T, the improvement is not predominately a consequence of the different volumes of the crystals. Hence, it is clearly observed that the diffracted intensity has improved. The 10 T and 0 T data sets can be scaled (using the program *SCALEIT* from *CCP*4), although the unit cell of the 10 T crystal did not change significantly (0.14–0.23%) compared with that of the 0 T crystal. The resulting R factor for agreement between 10 T and 0 T is 20.5% and the weighted R factor for agreement is 8.7%. These statistics compiled from the differences between the 10 T and 0 T data are useful in assessing the probability that the use of a high magnetic field of 10 T was responsible for the improvement in the quality of the 0 T crystal. Furthermore, if the mosaicity is reduced by 15–25%, the crystal quality should improve. Thus, although the conclusions regarding improved resolution limits are clear, the overall B factors estimated from the Wilson plot have lower values of 6 $Å^2$ in the 10 T case and 9 $Å^2$ in the 0 T case (Table 1) and the other statistics have been improved as shown in Table 3. These diffraction data largely support our observations pertaining to modest improvement in the higher resolution limit, reduced mosaicity and increased signal-to-noise ratio for the 10 T samples.

3.2. Protein structure comparisons

3.2.1. Overall. Each model was refined using data that led to a maximum resolution of 1.13 Å for 10 T and 1.33 Å for 0 T, *i.e.* truncated at the point where the average $I/\sigma(I)$ fell below

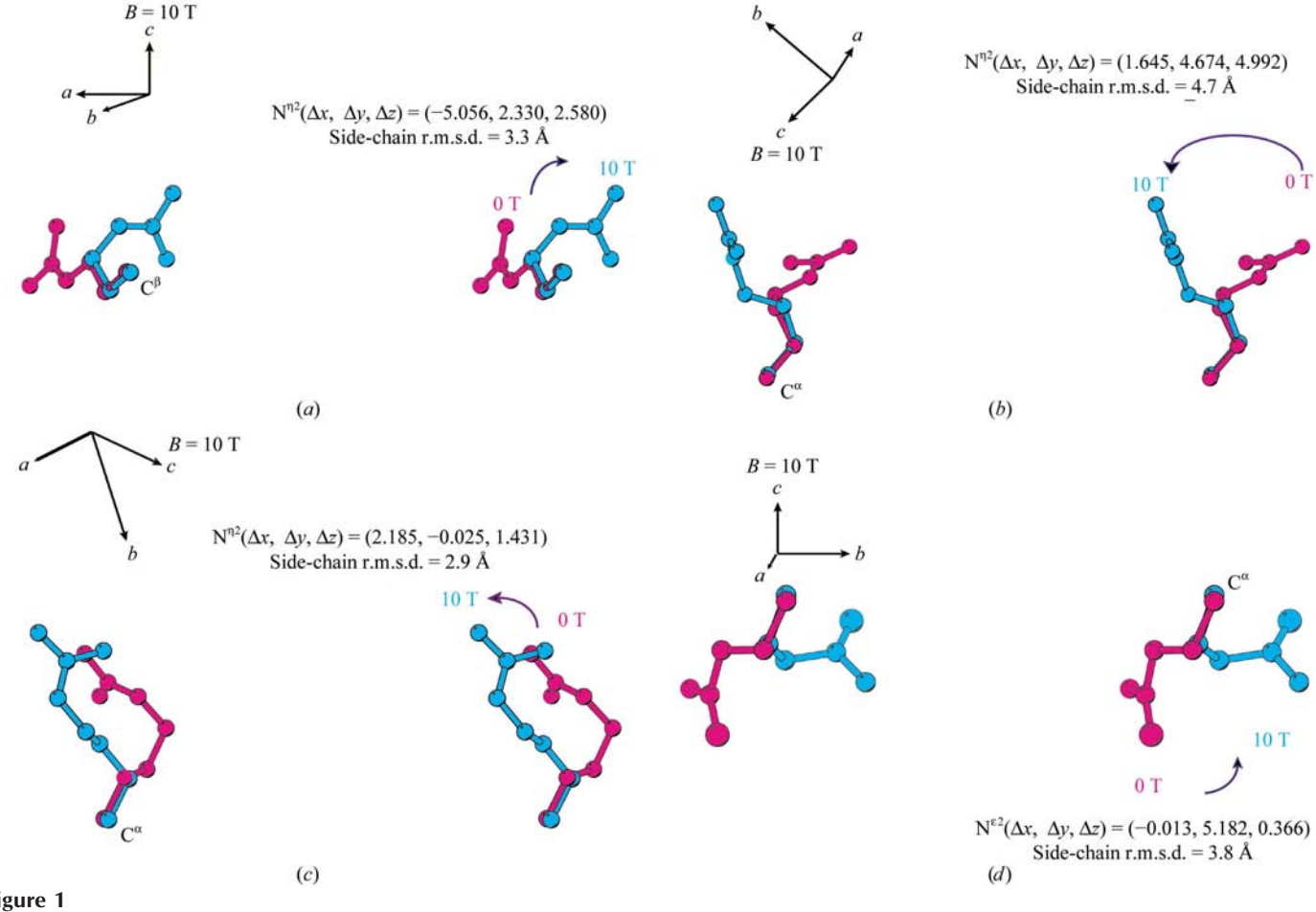

Figure 1
Stereoview of the superposition of side-chain conformations between the 10 T (blue) and 0 T (red) molecule. We focused on charged and polar residues with flexible and long side-chain structures, such as (*a*) Arg68, (*b*) Arg73, (*c*) Arg128 and (*d*) Gln121, in order to examine the effects of a magnetic field. The purple arrow indicates the displacement of the side chains; the C^{α} and C^{β} atoms are labelled. The displacement vector of the $N^{\eta 2}$ or $N^{\varepsilon 2}$ atom of these arginine and glutamine residues is defined as (Δx, Δy, Δz). The three axes indicated are in the orthogonal system in which the c axis direction was perpendicular to the high magnetic field. The figure was created using *BOBSCRIPT* (Esnouf, 1997) and *RASMOL*.

2.0. The lysozyme structures from the model refinements were compared. Both structures are high-quality structures, as evidenced from *PROCHECK* (Laskowski *et al.*, 1993), in terms of the positions of residues in the favoured and allowed regions of the Ramachandran plot (Table 3) and Luzzati plot (Luzzati, 1952), from which the estimated maximum average errors of 0 T and 10 T were found to be 0.16 and 0.18 Å, respectively. The r.m.s. deviations from ideal stereochemistry are 0.008 and 0.005 Å for bond lengths and 0.022 and 0.018° for bond angles, respectively. The model geometry residuals are also very good. Very subtle changes are observed that involve the movement of four or fewer residues between the allowed and favoured regions.

There are very few structural differences between the 10 T and 0 T forms of the protein. The r.m.s. differences on superposition of C^{α}, main-chain and all protein atoms of each structure were analyzed using *LSQKAB* (Kabsch, 1976) and we found that the final structures differed from one another by 0.75 Å. The protein structures are also very similar. Specifically, the two protein forms differ only in the surface loops or turns defined by amino-acid residues Arg68, Arg73 (on both sides of the type II turn 69–72), Gln121 (in the type III turn) and Arg128 (in the C-terminal amino-acid residues 126–129), which were roughly three times or more the r.m.s. deviation of all C^{α} atoms predicted by *LSQKAB*. The values obtained are listed in Table 4 and all show close agreement. Several amino-acid residues are present with well ordered side-chain densities including Arg68, Arg73, Gln121 and Arg128 (as partially shown in Fig. 1).

The guanidine groups of Arg68, Arg73 and Arg128 were displaced in the *ab*-plane direction by 5.6, 5.0 and 3.3 Å, respectively, which were larger than the displacements in the *c*-axial direction of 2.6, 5.0 and 1.4 Å, respectively. This evidence is sufficient to prove that the charged groups of the side chains were displaced by the Lorentz force in a direction perpendicular to the *c*-axial direction, which corresponds to the direction of the 10 T magnetic field. The distortions may also differ because these residues are located in the flexible turns or C-terminus, not the β-sheet and α-helix which have rigid secondary structure.

The amide group of Gln121 was also displaced by 5.2 Å in the *ab*-plane direction, which was larger by 0.4 Å than the displacement in the *c*-axial direction. In 10 T, Ser24 O was hydrogen bonded to the $O^{\varepsilon 1}$ atom of Gln121 with a distance of 3.1 Å and to the $N^{\varepsilon 2}$ atom of Gln121 with a distance of 2.7 Å. When a water molecule hydrogen bonds to Gln121 $N^{\varepsilon 2}$ (2.8 Å) and to Ser24 O (2.9 Å), both of these atoms have dipole moments, since they are polar residues. For 0 T, these two dipoles will interact in a manner similar to those of Ser24 and Gln121 observed for 10 T. However, Gln121 was not bound to any water molecules and, therefore, did not have an induced dipole, while the O^{γ} atom of Ser24 had an induced dipole *via* a water molecule that was hydrogen-bonded to this atom at a distance of 3.2 Å. Subsequently, a further dipole of Gln121 can be induced by electromagnetic induction, which causes interaction with a Ser24 dipole. In this case, the side chain of Gln121 may be displaced by the force exerted by the magnetic field. These structural 'consequences' of the magnetic effect are regarded as the Lorentz force and electromagnetic induction with a charge transfer. It is probable that the protein-folding state of 10 T may be more stable than that of 0 T owing to the formation of a new intramolecular interaction between Ser24 and Gln121.

Table 4
Displaced side chains defined by an overall significant deviation higher than 3σ.

Residue		R.m.s. deviation (Å)	Displacement	Å
Arg68	Main chain	0.33	In *ab* plane	5.6
	C^{α} atom	0.24	On *c* axis	2.6
	Side chain	3.31		
	$N^{\eta 2}$ atom	6.14		
Arg73	Main chain	0.11	In *ab* plane	5.0
	C^{α} atom	0.13	On *c* axis	5.0
	Side chain	4.78		
	$N^{\eta 2}$ atom	7.03		
Gln121	Main chain	0.09	In *ab* plane	5.2
	C^{α} atom	0.08	On *c* axis	0.4
	Side chain	3.76		
	$N^{\eta 2}$ atom	5.20		
Arg128	Main chain	0.14	In *ab* plane	3.3
	C^{α} atom	0.14	On *c* axis	0.9
	Side chain	2.88		
	$N^{\eta 2}$ atom	2.61		

3.2.2. Alternative conformations of charged side chains that disappear owing to the effect of a magnetic field. The 0 T structure included seven residues with disordered side chains (Arg21, Asn44, Ser86, Lys97, Val99, Val109 and Arg114), while the 10 T structure included only four residues (Asn44 in the β-sheet, Ser86 in the loop region and Val99 and Val109 in the α-helix) that formed alternative conformations. The conformational changes in the side chains of charged groups (Arg21 in the type II turn, Lys97 in the α-helix and Arg 114 at the carboxyl end) were not observed in 10 T. In the present model, inspection of the $(2|F_o| - |F_c|)$ maps indicated that the magnetic effect prevents any perturbation around the *c* axis of the side chain in arginine and lysine, which was also observed clearly in two distinct positions. In 0 T, the surface side chains of Arg21, Lys97 and Arg114 had structural disorder: the amino-acid side chains exhibited alternate conformations in two positions, 'A' and 'B'. In the 10 T magnetic field, no significant fluctuations were observed for the two conformations; one side-chain orientation of these residues is stabilized as position 'A' and position 'B' does not exist. Therefore, a high magnetic field has the ability to stabilize turns, α-helix or the C-terminus, making them more ordered.

In the 10 T case, alternate conformations of the four side chains at Asn44 (located in the antiparallel β-sheet), Ser86 (in the loop between the β-sheet and α-helix), Val99 and Val109 (in the α-helix) were observed. In 0 T, however, variations in the densities of multiple conformations in seven side chains at Arg21 (in the type II turn), Asn44, Ser86, Lys97 (in the α-helix), Val99, Val109 and Arg114 (in the type II′ turn) were observed. The electron density of Ser86, which starts this loop, suggests that this residue adopts multiple conformations at 0 T

and 10 T. The 10 T magnetic field allowed us to fix the charged side chains of three (Arg21, Lys97 and Arg114) of the seven amino-acid residues with disordered side chains at 0 T. The C-terminal amino-acid residue, Arg128, is disordered and cannot be seen clearly in the electron-density map of 0 T, but can be seen to be well ordered in 10 T. It has been noted that the neutral residues or internal side chains in a hydrophobic atmosphere are insensitive to the magnetic effect, since the dipole of the side-chain residues where the water molecule or charged ion is inaccessible cannot be induced by forming hydrogen bonds with a polar molecule.

3.3. Quantitative estimation from *B* factors

When comparing differences in *B* factors, the scaling process can correct the integrated intensity and compensate for the absorption anisotropy effects caused by a slightly differing crystal shape. The small ΔB values between 10 T and 0 T were observed using the same refinement software, which had a superior sensitivity to these *B* factors, using a common procedure. However, the *B* factors for the protein atoms have values of 17.8 and 19.5 Å^2 in the 10 T and 0 T structures, respectively, *i.e.* a ΔB of 1.7 Å^2 in favour of the 10 T structure. The differences between the main-chain protein atom *B* values are 16.4 Å^2 for the 10 T case and 17.9 Å^2 for the 0 T control, *i.e.* a ΔB of 1.5 Å^2. The largest differences between side-chain protein atom *B* values are 19.3 Å^2 for the 10 T case and 21.1 Å^2 for the 0 T control, *i.e.* a ΔB of 1.8 Å^2.

All the waters in the 114 and 87 molecules studied had an average *B* factor of 37.8 and 34.6 Å^2 in the 10 T and 0 T cases, respectively, *i.e.* a ΔB of 3.2 Å^2 in favour of the 0 T structure. Of these, 74 common waters had an average *B*-factor value of 33.4 Å^2 for 10 T and 32.9 Å^2 for 0 T. The marked differences between the *B* factor of the chloride ion are 7.7 Å^2 for 10 T and 5.4 Å^2 for 0 T, *i.e.* a ΔB of 2.3 Å^2 in favour of 0 T as described above. Furthermore, it was considered that the *B* factor of the Na atom might be too large to be observed. As a structural characteristic of the magnetically oriented lysozyme, it was found that as the *B* factor of bound water molecules or ionized chloride ions becomes larger, the *B* factor of spatially bulky protein atoms becomes smaller. As far as the solvent portion of the water molecules or ionized atoms is concerned, these larger *B* values increase in the 10 T case. Although the changes in *B* factors are small because of the similar values of scattering for water molecules and ions such as sodium and chloride, the changes are nevertheless unfavourable in the case of the 10 T structure. Contrary to expectation, a larger *B*-factor value was seen for the chloride ion with which a hydrogen bond is formed between the main chain of Ser81 and the side chain of Arg125 in adjacent molecules in 10 T. Relatively long intermolecular distances have been observed for Cl$\cdots$Ser81 N, with a bond distance of 0.08 Å, and Cl$\cdots$Arg125 N$^{\eta}$ with a bond distance of 0.12 Å and molecular contacts have been weak. These results suggest that an ion such as chloride can exchange rapidly with water molecules. It is likely that the high magnetic field of 10 T may be able to improve the quality of protein crystals by way of an intermolecular bound solvent, although the changes would be small. However, neither a small quantity of bound water nor ions are disordered in the hydration structure of 10 T, despite the higher resolution. Therefore, the bound water molecules, cationic ions and anions affected by a magnetic field may not contribute greatly to the improvement of crystal quality, even though these consist of the same diamagnetic materials as the protein.

The overall average temperature factors for the common atoms have values of 19.9 and 20.7 Å^2 for 10 T and 0 T, respectively. A *B*-factor improvement of 0.8 Å^2 is observed for 10 T over its 0 T control for molecular atoms located in common positions. According to the definition provided in (1), this corresponds to a 22.6% improvement in data intensity at a 1.33 Å resolution, as estimated from $[(\sum_{10\,\mathrm{T}} - \sum I_{0\mathrm{T}})/I_{0\mathrm{T}}] \times 100$. In addition, compared with 604 equivalent reflections from the 10 T crystal observed in the 0 T outer resolution shell between 1.38 and 1.33 Å, the averaged intensity exhibited an increase of 37.7%, contrary to the reduction of 11% in the volume of the 10 T crystal compared with that of the 0 T crystal.

As shown in Table 5, protein atoms comprise 93.2% (content of atoms *n*) of the atoms in the crystal. They contributed to a 97.9% ($\Delta I_{\mathrm{partial}} \times 100/\Delta I_{\mathrm{overall\ atom}}$) increase in the diffracted intensity. A portion of the protein molecule made a contribution to the improvement in the diffracted intensity of 1.05 ($\Delta I_{\mathrm{partial}}/n\Delta I_{\mathrm{overall\ atom}}$) per atom, which was estimated to be similar to that for a main chain (1.07) and a side chain (1.05). There were 74 common bound waters conserved between the 10 T and 0 T structures. Since conserved waters comprised 6.8% of all ordered atoms in the 10 T crystal, the overall diffraction intensity of the crystal increased by 0.9% at 1.33 Å compared with the 0 T case. The waters found in common positions did not contribute greatly to enhancing the diffraction intensity in the 10 T case. The contribution to the diffraction intensity was estimated to be a slight increase of 0.13 over the 0 T control.

A larger difference in the change of intensity value is observed in the protein atoms by taking into account the number of constituent atoms in a crystal. Thus, in improving the quality of crystals, a high magnetic field affects the whole protein molecule rather than the bound water.

It was believed that the magnetic susceptibility of the protein would be maintained because there was no change in the main-chain structure except for a lowering of the *B* factor. Although this was expected to be caused by the diamagnetic anisotropy of peptide planes in the main chain and the aromatic rings in the side chains of the protein molecule (Worcester, 1978), neither main chain nor side chains with decreased *B* factors were clearly observed. However, the chain structure was susceptible to a reduction in the *B* factors of the molecule on the whole rather than specific local portions of protein and solvent ions. The magnetic effects on the depression of the *B* factor are not sharply differentiated between β-sheet, α-helix and turn, which includes loop portions and both the N- and C-termini.

Table 5
B-factor analysis of atoms common to the 10 T and 0 T structures.

The improvement rate of the diffracted intensity is calculated from the *B*-factor difference for the protein portion of the crystal. Using (1), the improvement factor of each portion is shown as the increase in its diffraction intensity at 1.33 Å.

	No. common atoms *N*	Difference in estimated diffraction intensity†	Fractional intensity change‡ (%)	Increases in the intensity of partial structure to overall atoms§ (%)	Content of atoms in crystal, *n* (%)	Contribution to improvement rate¶
Overall	1083	2.35	22.6	100	100	1
Protein	1009	2.3	22.5	97.9	93.2	1.05
Main chain	516	1.2	17.7	51.1	47.7	1.07
Side chain	493	1.12	27.1	47.7	45.5	1.05
α-Helix	275	0.53	13.2	22.6	25.4	0.89
β-Sheet	78	0.33	30.3	14.0	7.2	1.94
Turn *etc.*	656	1.45	28.7	61.7	60.6	1.02
Bound water	74	0.02	22.2	0.9	6.8	0.13

† $\Delta I = \sum I_{10\,\mathrm{T}} - \sum I_{0\,\mathrm{T}}$. ‡ $[(\sum I_{10\,\mathrm{T}} - \sum I_{0\,\mathrm{T}})/\sum I_{0\,\mathrm{T}}] \times 100$. § $(\Delta I_{\mathrm{partial}}/\Delta I_{\mathrm{overall}}) \times 100$. ¶ $\Delta I_{\mathrm{partial}}/(n\Delta I_{\mathrm{overall}})$.

3.4. Conformational energy searching for the dihedral angle

Significantly, the 10 T and 0 T protein forms differ only in the surface loops or turns defined by amino-acid residues Arg68, Arg73 (on both sides of the type II turn 69–72), Gln121 (in the type III turn) and Arg128 (in the C-terminal amino-acid residues 126–129). A comparison of the *B* values for these forms showed that the *B* factors of these four residues were lowered by 5.1–9.3 Å^2 for the main chains and of 4.3–8.4 Å^2 for the side chains, respectively. Small displacements, such as in alternate side-chain conformations, can occasionally be identified in seven residues, Arg21 (in the type II turn), Asn44 (located in the antiparallel β-sheet), Ser86 (in the loop from the β-sheet to the α-helix), Lys97 (in the α-helix), Val99 (in the α-helix), Val109 (in the α-helix) and Arg114 (on the type II′ turn), in the 0 T structures and four residues, Asn44, Ser86, Val99 and Val109, in the 10 T structures. Only the charged group of the three inner amino acids Arg21, Lys97 and Arg114 exhibit fixed conformations. Moreover, comparisons of *B* values for these proteins show that the *B* factors of charged side chains were lowered. The magnetic effect of the charged amino acids was confirmed by the disappearance of the alternate conformation of the three residues, since their alternate side-chain conformations remain for four uncharged residues, Asn44, Ser86, Val99 and Val109, in the 10 T structure.

Residues such as arginine (guanidine) and lysine (ε-NH_2), histidine (imidazole) and amino-acid α-NH_2 are completely positively charged since they are in a crystallization medium of pH 4.5. This results in a considerable change in the conformation of the side chain of the basic amino acid on the protein surface, which is inferred from the Lorentz effect.

The acidic residues are also expected to be inactive even against a high magnetic field since Glu and Asp residues lose their negative charge at acidic pH. The external side-chain dihedral angles respond more sensitively than the main-chain peptide angle to high magnetic field owing to the order of increasing flexibility: the main chain of helices and sheets, the entire main chain, internal side chains and external side chains. The energy of each conformation is determined by a mechanics calculation without optimization using augmented MM3 parameters. Non-optimized rigid maps are useful for investigating how energy changes as a function of specific geometry attributes in the molecules under consideration. The representative change in the dihedral angle of the side chain in basic residues such as Arg68 and Lys97 is reported in Figs. 2(*a*) and 2(*b*), respectively. For example, the side chains of an arginine residue have χ_1 (C–C$^\alpha$–C$^\beta$–C$^\gamma$), χ_2 (C$^\alpha$–C$^\beta$–C$^\gamma$–C$^\delta$), χ_3 (C$^\beta$–C$^\gamma$–C$^\delta$–N$^\varepsilon$) and χ_4 (C$^\gamma$–C$^\delta$–N$^\varepsilon$– C$^\zeta$); each χ approximates a staggered conformation. In these energy diagrams, the high magnetic field imposes an energy change between 10 T (solid line) and 0 T (dotted line). The energy diagram for a given conformation, which is derived from the significant r.m.s. deviation of its corresponding side chains in the two crystal structures, can be used to explore the full range of conformational space and to subsequently find the shallow minima and the shelf of the energy function.

Disregarding the high magnetic field, conformational energy searching in molecular mechanics may provide some physical meaning for the difference in the energies of the side-chain dihedral angles corresponding to the 0 T and 10 T structures. The energy conformations of 10 T are in general lower than those of 0 T. The difference in molecular-mechanics energy can be estimated to be -598 kJ mol^{-1} for Arg68, -473 to -343 kJ mol^{-1} for Lys97, -582 kJ mol^{-1} for Gln121, -628 kJ mol^{-1} for Arg73 and -593 kJ mol^{-1} for Arg128. It is suggested that the 10 T magnetic field may change the potential energy diagram and may contribute to stabilizing the energetically preferred conformation, which is not located at the minima of its energy function. The conformation at 10 T can lead to the local minimum, so that the charged side chain may be subjected to forces such as the Lorentz force, which is applied when a high magnetic field is employed.

3.5. Anisotropic mosaicity

Seven of the 10 T crystals had an average η of 0.0054° with a standard deviation of 0.0007°. The 0 T crystals of the same number had an average η value of 0.0078° (with a standard deviation of 0.0012°). This η value was 1.4 times higher than that of the 10 T crystals and the 0 T crystals possessed poor

diffraction power. The η values for 56 individual reflections varied over a large range, with standard deviations of between 0.0003 and 0.0009°. The spread in η for 10 T crystals was 1.7-fold narrower, with standard deviations ranging from 0.0001 to 0.0005°. Using the regression analysis for all measured FWHM values and according to the definition provided in (2), the mosaicity values of η_h, η_k and η_l for the 10 T crystals were 0.0065, 0.0049 and 0.0048°, respectively. On the other hand, the mosaicity values for 0 T were 0.0084, 0.0078 and 0.0069°, respectively. The isotropic nature of the mosaicity was reduced for the 0 T crystal, with the anisotropic

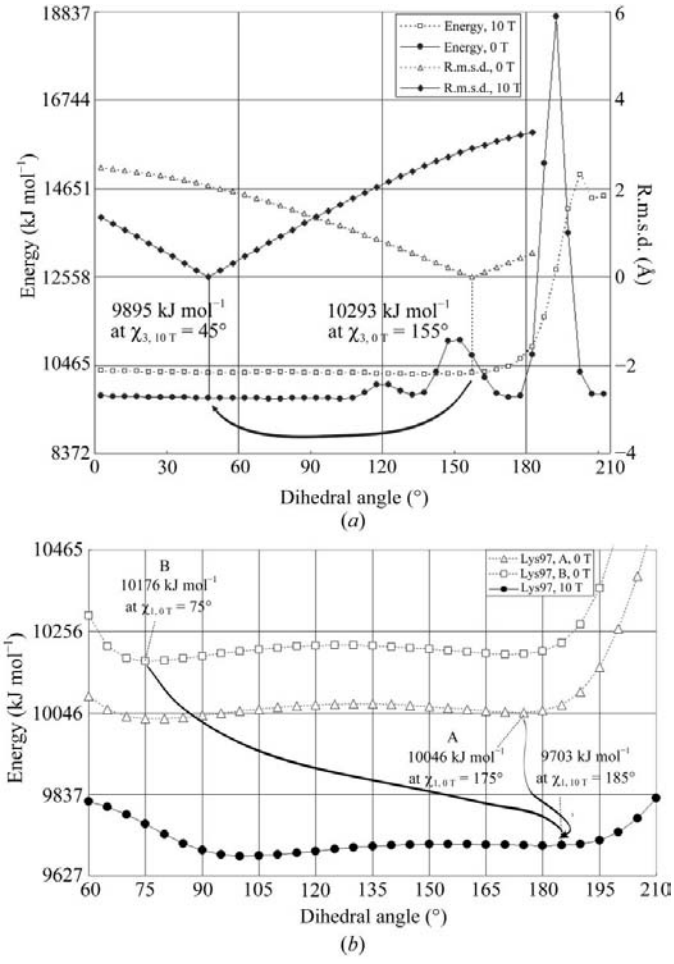

Figure 2
Systematic energy search for deformation of the dihedral angle induced by high magnetic field. The potential energy of the resulting conformations is plotted against a dihedral angle with a 5° stepwise rotation for specified side-chain components. (*a*) With the dihedral angle χ_3 in the side chain of Arg68, it was specified that a range of rotations from 0 to 360° with a stepwise rotation of 5° be sampled. The spin around 110° of 10 T was so favourable that 0 T may be met with the peak of conformation energy as a consequence of destabilization induced by the high magnetic field of 10 T. (*b*) The dihedral angle χ_1 in the side chain of Lys97. The two conformations of 0 T (squares and triangles) may result in two local minimas that nestle into the foot of the highest energy barrier. The optimum $\chi_{1,\,0\,T}$ = 75 or 175° are confirmed in the crystal structure. However, the shelf-like surface of 10 T (circles) illustrates how convergence can occur before reaching the minimum energy of $\chi_{1,\,10\,T}$ = 100°. The conformation can lead to a local minimum of $\chi_{1,\,10\,T}$ = 185° so that the charged side chain may be subjected to a high magnetic field of 10 T.

mosaicity arising from the 10 T magnetic effect, with 0.4, 0.5 and 1.0% Å^{-1} along the *a*, *b* and *c* axes, respectively. Inspection of the mosaicity values and their indices shows that the change of mosaicity was large with respect to resolution. (To fit a linear model, the multiple correlation coefficient of regression analysis was R = 0.919 and the corresponding R^2 was 0.844.) The values of the average anisotropic mosaicity reduce to 0.0019, 0.0029 and 0.0021°, respectively.

The relative contributions from angular misalignment of mosaic blocks and the volume can be distinguished from those from mosaicity arising from lattice strains (the variation of *d* spacing within a mosaic block) owing to lattice defects or impurity incorporation. The contributions can be understood by studying mosaicity as a function of resolution. The angular misalignment of mosaic blocks and the volume effects are independent of resolution, whereas mosaicity arising from lattice strains is dependent on resolution. If the mosaicity increases as a function of resolution, then we can conclude that the lattice strains are significant. The resolution contribution in a high magnetic case was observed to be minimal; hence, the main effects on mosaicity are governed by the volume of the mosaic block size and the angular misalignment of the mosaic blocks in an array (which is the most obvious disorder). The volume then becomes very large, which may be caused by homogeneous formation of the mosaic blocks in the crystal.

It is suggested that the lattice errors cause local (impurities) or extended (such as line or plane) dislocations; therefore, a tilt angle develops between two mosaic blocks (Shaikevitch & Kam, 1981). A dislocation results from the accumulation of lattice errors in the unit cell and is used to estimate the volume of the mosaic block size. Systematic errors are linearly proportional to the N unit cells, while random errors grow in each direction as the square root of the N unit cells. Fitting this systematic error model to the calculated value of the anisotropic mosaic spread of 10 T gives an average mosaic block with dimensions of 50, 85 and 35 µm along the *h*, *k* and *l* axes, respectively. The volume was 150 × 10^3 µm^3. Similarly, the dimensions of the mosaic block size of the 0 T crystal are 40, 55 and 25 µm and its volume is 55 × 10^3 µm^3. Therefore, the mosaic block of the 10 T crystal appears to be about three times the size of that of the 0 T crystal. The average mosaic block of the 0 T *versus* 10 T cases increases by 25, 55 and 40% along the *a*, *b* and *c* axes, respectively. The *b* direction corresponds to the longest unit-cell parameter and also has a twofold screw axis. The direction of highest perfection, therefore, lies orthogonal to the direction of favoured growth, which becomes magnetically oriented. The mosaic block of the 0 T crystal consisted of 6800 × 7300 × 8200 = 4 × 10^{11} lysozyme molecules. The 10 T crystal blocks are three times the size of the 0 T crystal blocks, consisting of 8800 × 11500 × 11500 = 12 × 10^{11} molecules. As Yanagiya *et al.* (1999) predicted that it is necessary to aggregate at least 7 × 10^4 molecules, the minimum size of the magnetically oriented crystal is found to be 90 nm for 10 T. For example, when the magnetic stabilization energy of crystals exceeds their thermal fluctuation energy, the crystals become magnetically oriented,

aligning their *c* axis in the direction of the magnetic field. Hence, the magnetic orientation (under a provided magnetic field) is not only expected for all the crystals but is also shown to be sufficient to orient an even smaller portion than the mosaic block in the crystal. Thus, we demonstrated the beneficial effect of the magnetic field on the X-ray diffraction intensities under the decreased mosaicity that leads to increased mosaic block size. Molecular orientation is responsible for the improvement in the quality of a protein crystal in a high magnetic field.

The reason for the improvement in crystal quality using a magnetic field may be the orientation effect of the high magnetic field. Therefore, crystal mosaicity was decreased in reciprocal space by the larger volume and smaller angular misalignment of the mosaic blocks, with the most obvious effects at the maximum resolution limit in the signal-to-noise ratio of intensity and in the reduced mosaicity.

4. Concluding remarks

In order to develop a rational approach for obtaining better diffracting protein crystals, we have initiated studies on small globular proteins, such as HEW lysozyme, where crystallization takes place in a high magnetic field. The quality of orthorhombic lysozyme crystals formed under a uniform 10 T magnetic field was indeed found to be superior to the quality of 0 T crystals (*i.e.* crystals formed in the absence of a magnetic field). A comparative analysis of the two crystal structures has revealed that overall the 10 T structure remains very similar to the 0 T structure. Put another way, there seemed to be no overall significant impact on the protein structure for the crystal grown in the high magnetic field. However, there were interesting rationalizable differences in specific amino acids owing to the high magnetic field during crystal growth, the effect of which on protein crystallization can be summarized as follows. (i) Arginine and lysine residues from the main chain located on a flexible loop were displaced. (ii) There was a reduction in alternative conformations for amino acids with bulky or longer side chains with an electric charge such as arginine or lysine. Residues such as arginine (guanidine), lysine (ε-NH_2), histidine (imidazole) and amino acid α-NH_2 are completely positively charged since they are in a crystallization medium of pH 4.5 and this results in a considerable change in the conformation of the side chain of the basic amino acid on the protein surface inferred from the magnetic Lorentz effect. On the other hand, it is probable that for cases of either uncharged acidic residues, such as amino acid α-CO_2H, glutamine (CO_2H) and aspartic acid (CO_2H), *i.e.* those that are almost certainly protonated below pH 4.5, will not be sensitive to the magnetic field. If displacements of residues on the structure arise as a consequence of receiving Lorentz force and electromagnetic induction caused by the high magnetic field, it can be considered that the crystal quality may be improved by the magnetic orientation of protein molecules as well as nuclei. It is possible that an evenly distributed magnetic field of 10 T gives a sufficiently large magnetic energy for the orientation. By anisotropic mosaicity analysis, the mosaic block size of the crystals grown in a high magnetic field was three times larger compared with that of the control crystals. Consequently, the 10 T crystals that were taken on to full structure refinement yielded a more homogeneous structure. The diffracted intensity increase of 37.7% which was observed in the experiment was compared with a 22.6% increment estimated theoretically from the average *B*-factor analysis calculated by subtracting the contributory shares of conformation energy. In order to examine whether the displacement is energetically favourable, we have also performed theoretical calculations on the conformational changes in the side chains of basic residues. Since a field of 10 T contributes to the stability of the dihedral angle by -578 kJ mol^{-1} per charged residue, it was possible to ascertain that the effect of a magnetic field in crystallization is applicable to any protein, *i.e.* its use is not restricted to haem proteins. The field may actually help in obtaining better quality protein crystals that have so far resisted forming ordered arrays. However, there is little doubt regarding the fact that magnetic enhancement in crystal perfections is an important material engineering tool in the study of protein structure and function.

This study was carried out as a part of the 'Ground Research Announcement for Space Utilization' promoted by NASDA and the Japan Space Forum. This work was partly supported by the Grant of the 21st Century COE Program and Grant-in-Aid for Scientific Research (C) from the Japanese Ministry of Education, Culture, Sports, Science and Technology. We are also grateful for the facilities used and assistance of the staff at the High Field Laboratory for Superconducting Materials, Institute for Materials Research, Tohoku University, Japan. This work was performed with the approval of the Photon Factory Advisory Committee, Japan (proposal No. 2000G-316). TS and NT are members of the SBSP project of High Energy Accelerator Research Organization, Tsukuba, Japan. The authors wish to express their sincere thanks to the staff at the Photon Factory for their help with data collection.

References

Astier, J. P., Bokern, D., Lapena, L. & Veesler, S. (2001). *J. Cryst. Growth*, **226**, 294–302.
Ataka, M. & Wakayama, N. I. (2002). *Acta Cryst.* D**58**, 1708–1710.
Bellamy, H. D., Snell, E. H., Lovelace, J., Pokross, M. & Borgstahl, G. E. O. (2000). *Acta Cryst.* D**56**, 986–995.
Colapietro, M., Cappuccio, G., Marciante, C., Pifferi, A., Spagna, R. & Helliwell, J. R. (1992). *J. Appl. Cryst.* **25**, 192–194.
Collaborative Computational Project, Number 4 (1994). *Acta Cryst.* D**50**, 760–763.
Cruickshank, D. W. J. (1999). *Acta Cryst.* D**55**, 583–601.
Czepas, J., Devedjiev, Y., Krowarsch, D., Derewenda, U., Otlewski, J. & Derewenda, Z. S. (2004). *Acta Cryst.* D**60**, 275–280.
Derewenda, Z. S. (2004). *Structure*, 12, 529–535.
Esnouf, R. (1997). *J. Mol. Graph.* **15**, 133-138.
Ferrer, J. L. & Roth, M. (1998). *J. Appl. Cryst.* **31**, 523–532.
IUPAC-IUB Conventions (1972). *J. Mol. Biol.* **50**, 1.
Habash, J., Boggon, T. J., Raftery, J., Chayen, N. E., Zagalsky, P. F. & Helliwell, J. R. (2003). *Acta Cryst.* D**59**, 1117–1123.

Kabsch, W. (1976). *Acta Cryst.* A**32**, 922–923.
Kissinger, C. R., Gehlhaar, D. K. & Fogel, D. B. (1999). *Acta Cryst.* D**55**, 484–491.
Laskowski, R. A., MacArthur, M. W., Moss, D. S. & Thornton, J. M. (1993). *J. Appl. Cryst.* **26**, 283–291.
Lin, S. X., Zhou, M., Azzi, A., Xu, G. J., Wakayama, N. & Ataka, M. (2000). *Biochem. Biophys. Res. Commun.* **275**, 274–278.
Luzzati, P. V. (1952). *Acta Cryst.* **5**, 802–810.
Mateja, A., Devedjiev, Y., Krowarsch, D., Longenecker, K., Dauter, Z., Otlewskib, J. & Derewenda, Z. S. (2002). *Acta Cryst.* D**58**, 1983–1991.
Oki, H., Matsuura, Y., Komatsu, H. & Chernov, A. A. (1999). *Acta Cryst.* D**55**, 114–121.
Otwinowski, Z. & Minor, W. (1997). *Methods Enzymol.* **276**, 307–326.
Press, W. H., Flannery, B. P., Teukolsky, S. A. & Vetterling, W. T. (1995). *Numerical Recipes in C: The Art of Scientific Computing*, pp. 681–688. Cambridge University Press.
Roussel, A. & Cambillau, C. (1989). *Silicon Graphics Geometry Partner Directory.* Silicon Graphics, Mountain View, CA, USA.
Sato, N., Uragami, T., Nishizaki, T., Takahashi, Y., Sazaki, G., Sugimoto, K., Nonaka, T., Masai, E., Fukuda, M. & Senda, T. (2002). *J. Mol. Biol.* **321**, 621–636.
Sato, T., Hara, S., Matsui, T., Sazaki, G., Saijo, S., Ganbe, T., Tanaka, N., Sugano, Y. & Shoda, M. (2004). *Acta Cryst.* D**60**, 149–152.
Sato, T., Yamada, Y., Saijo, S., Hori, T., Hirose, R., Tanaka, N., Sazaki, G., Nakajima, K., Igarashi, N., Tanaka, M. & Matsuura, Y. (2000). *Acta Cryst.* D**56**, 1079–1083.
Sato, T., Yamada, Y., Saijo, S., Hori, T., Hirose, R., Tanaka, N., Sazaki, G., Nakajima, K., Igarashi, N., Tanaka, M. & Matsuura, Y. (2001). *J. Cryst. Growth*, **232**, 229–236.
Sazaki, G., Durbin, S. D., Miyashita, S., Ujihara, T., Nakajima, K. & Motokawa, M. (1999). *Jpn J. Appl. Phys.* **38**, 842–844.
Shaikevitch, A. & Kam, Z. (1981). *Acta Cryst.* A**37**, 871–875.
Snell, E. H., Bellamy, H. D. & Borgstahl, G. E. O. (2003). *Methods Enzymol.* **368**, 268–288.
Snell, E. H., Cassetta, A., Helliwell, J. R., Boggeon, T. J., Chayen, N. E., Weckert, E., Hölzer, K., Schroer, K., Gordon, E. J. & Zagalsky, P. F. (1997). *Acta Cryst.* D**53**, 231–239.
Snell, E. H., Judge, R. A., Crawford, L., Forsythe, E. L., Pusey, M. L., Sportiello, M., Todd, P., Bellamy, H. D., Lovelace, J., Cassanto, J. M. & Borgstahl, G. E. O. (2001). *Cryst. Growth Des.* **1**, 151–158.
Worcester, D. L. (1978). *Proc. Natl Acad. Sci. USA*, **75**, 5475–5477.
Yanagiya, S., Sazaki, G., Durbin, S. D., Miyashita, S., Nakajima, K., Komatsu, H., Watanabe, K. & Motokawa, M. (1999). *J. Cryst. Growth*, **196**, 319–324.
Zhong, C. & Wakayama, N. I. (2001). *J. Cryst. Growth*, **226**, 327–332.